Simultaneous triple imaging with two PARASHIFT probes: encoding anatomical, pH and temperature information using magnetic resonance shift imaging

Katie-Louise N. A. Finney[a], Alice C. Harnden[a], Nicola J. Rogers[a], P. Kanthi Senanayake[a], Andrew M. Blamire[b], Dara O'Hogain[b] and David Parker[a]*

a) Department of Chemistry, Durham University, South Road, Durham DH1 3LE, UK.

b) Institute of Cellular Medicine & Newcastle MR Centre, Newcastle University, Newcastle upon Tyne, NE4 5PL, UK.

E-mail: ***david.parker@dur.ac.uk*** . Supporting information and ORCID(s) from the author(s) for this article are available on the www under ***http://dx.doi.org/10.1002/chem.***xxxxxxxxx

Abstract: The chemical shift of paramagnetically shifted resonances in lanthanide(III) complexes encodes information about temperature and has also been made to report pH in parallel, through introduction of a single phosphonate group adjacent to the reporter *t*-butyl resonance. The enhanced sensitivity of this new probe has allowed the simultaneous triple imaging of the water signal and the shifted *t*-butyl signals of thulium and dysprosium complexes of a common ligand, separated by over 160 ppm. In parallel spectral imaging experiments, the temperature and pH dependence of the frequency of the Tm and Dy signals has been deconvoluted, allowing the pH and temperature in the liver, kidney and bladder to be measured.

Introduction

We introduce a spectroscopic imaging system that allows the spatial distribution of water to be assessed at the same time as mapping local tissue temperature and pH, using two paramagnetic complexes of the same ligand.

Proton magnetic resonance spectroscopy *in vivo* is an inherently insensitive method that has remained far less exploited than MRI, but offers the opportunity to identify and map metabolic and physiological processes via the chemically shifted resonance of species other than water. Both endogenous species and added probes normally need to be present in the millimolar concentration regime to be detected quickly, over the magnetic field range 1.5 to 7

T. On the other hand, the abundant local water signal resonating around 4.7 ppm can be very quickly observed, and both its varying local concentration and differing longitudinal relaxation time in different tissue types allows valuable image contrast to be obtained. [1,2] There are two coupled practical problems inhibiting co-observation of the water signal and other proton signals *in vivo*. First, the endogenous or probe signal needs to be enhanced, and hyperpolarisation techniques have shown considerable promise, notwithstanding their short duration.[3] Another means of enhancing signal intensity per unit time involves paramagnetic relaxation, wherein a faster relaxing probe signal can be observed with a 15 to 25 times increase in intensity versus diamagnetic controls, using fast pulsed NMR techniques. [4-6] Second, the observed signal should be shifted well away from the water and fat signals to allow it to be observed separately, requiring a very large sweep width to be used with very short repetition times, without the need for water suppression. At a field of 7 T (300 MHz), the signal should resonate about 15 to 20,000 Hz away from the water/fat signals, i.e. beyond ±50/60 ppm, (*Scheme 1*).

Paramagnetic probes based on the fast-relaxing lanthanide(III) ions offer solutions to these problems. To improve sensitivity they can be labelled with homotopic ^{t}Bu groups that undergo fast relaxation in the range 80 to 150 s^{-1}, over the field range 1 to 7 Tesla. The ^{t}Bu resonance, when it is located about 6.6 Å from the metal ion in an 8-coordinate complex, can be tuned to resonate ±80 ppm from the water signal, by varying the Ln^{3+} ion. [7,8] By selecting the lanthanide ion from the series of five 'fast-relaxing' and 'large-shifting' rare-earth ions (Tb, Dy, Ho, Er and Tm) according to the magnetic field to be used, it is possible to select a pair of complexes with similarly large, but opposite paramagnetic shifts and similar R_1 and R_2 values. Such features allow the implementation of a common pulse sequence to simultaneously and *directly* observe each resonance. Moreover, in addition to a very large temperature sensitivity of the observed chemical shift, responsiveness to local pH change can be engineered (or in principle, sensitivity to pM), by introducing an ionisable group that protonates between pH 5 and 8, perturbing the reporter resonance frequency. [9-11a] We emphasise here the fundamental difference between our approach using paramagnetic shift and increased relaxivity to enhance the molecular MR signal from the complex itself, as opposed to other indirect detection approaches, whereby the interaction between complex and solvent (tissue water) is detected (e.g. CEST methodology).

Altered extracellular pH *in vivo* is associated with chronic diseases, such as end stage renal failure and coronary artery disease, as well as in the tissue ischemia associated with many cancers. There are very few non-invasive markers used clinically to quantify pH in deep

tissue. [11] There is a degree of uncertainty about the pH of the kidney due to difficulties in calibration [11b] : Gillies using the pH-dependence of Gd complex relaxivity changes, suggested pH values as low as 6.3 in the calyx, whereas the cortex and medulla are believed to be higher. More recent data [11c] also suggests values of 7.3, 7.0 and 6.6 for the cortex, medulla and calyx respectively, dropping by 0.2 pH units in the 'acidotic' disease states that typify renal failure. Similarly, elevated local temperatures are often associated with inflammation, notably in hepatitis and in liver and kidney fibrosis. The systems here, i.e. based on $[Ln.L^{1a}]^-$ have pK_a values (50% aq. serum, *vide infra*) of 6.7: these are well suited to the clinical need.

With these issues in mind, we have developed the series of complexes, $[HLn.L^1]^-$ (*Scheme 1*) in which the lanthanide ion is Tb, Dy, Ho, Er or Tm. The ligand structure incorporates an arylphosphonate group, with a pK_a value in the region of 7, according to the local ionic strength, solvent polarity and temperature. Phenylphosphonic acid itself has been studied by ^{31}P magnetic resonance as an *in vivo* pH probe in magnetic resonance spectroscopy. [12]

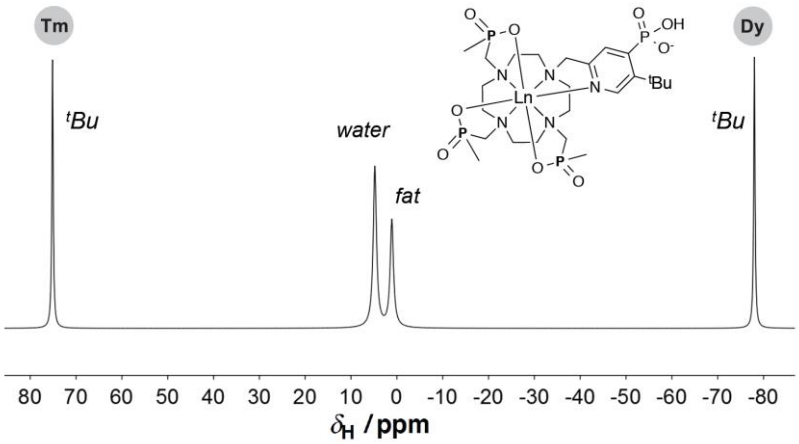

Scheme 1.

Using two complexes of the same ligand, e.g. Tm(III) and Dy(III), the dual pH/*T* dependence of the observed chemical shift can be resolved, provided that the intrinsic pH and *T* dependence of the shift for each complex is known, under the conditions found *in vivo*. Therefore, by consecutively exciting each well-separated resonance within a brief pulse delay (compared to T2), a spectroscopic imaging experiment can be devised, observing the water signal and the two ^{t}Bu probe resonances by dual excitation, in *the same* acquisition period.

Pulse sequences that can be used to acquire data on two or more resonances simultaneously have been developed some time ago. [13] Coman has studied the behaviour of $[Tm.DOTMA]^-$ and the pH sensitive complex $[Tm.DOTP]^{5-}$, examining multiple frequencies that were very well shifted on either side of the water signal.[14,15] A process of interleaved acquisitions was used, representing a reduction in sensitivity, as they were effectively running at a longer

(double) repetition time, T_R. In that case, the very widely separated 4H reporter signals (~26,000 Hz at 500 MHz) had short T_1 and T_2 values of 1 and 0.5 ms respectively, that may have made the concept of a dual excitation experiment not feasible, at that time. These important studies were carried out in nephrectomised animals, using a continuous infusion of the complex and operated at a field of 11.7 T, in order to get sufficient sensitivity to observe the rather broad signal. The use of this surgical approach raises and artificially maintains a high blood concentration of complex, such that in a rat model, complex passed the blood-brain-barrier and it was possible to measure the distribution of pH from individual voxels across the entire rat brain. More recently, Huang has extended that work to use a more efficient dual-band excitation pulse which simultaneously detects the dual frequencies of the $[Tm.DOTP]^{5-}$ complex and evaluated the use of an organic anion transporter inhibitor (probenecid) to slow excretion of the agent **[15b]**. In the work reported herein, imaging studies were undertaken using a normal, intact mouse model, with a single tail-vein injection of 0.04 mmoles/kg and with no attempt to alter natural excretion rates. A single pulse train was used to create a simultaneous triple imaging experiment of agents and water, for the first time.

Results and Discussion

The synthesis of the target complexes, $[HLn.L^1]^-$ was undertaken using a convergent route in which the key heterocyclic moiety was introduced late in the scheme by an alkylation reaction at the fourth ring nitrogen position (Schemes 2 and 3). Nitration of 3-*t*-butyl-6-methyl pyridine N-oxide [7] gave the 4-nitro derivative, **1**, and stepwise reduction, diazotization and trapping of the aryldiazonium ion with iodide, afforded the *p*-iodo derivative, **3**. Thermolysis in acetic anhydride led to functionalisation of the proximate benzylic site generating the acetate ester, **4**. Palladium catalysis of C-P bond formation using $P(OEt)_3$, [16] followed by selective base hydrolysis of the carboxylate ester, gave the primary alcohol, **6**, from which the mesylate, **7**, was prepared under standard conditions.

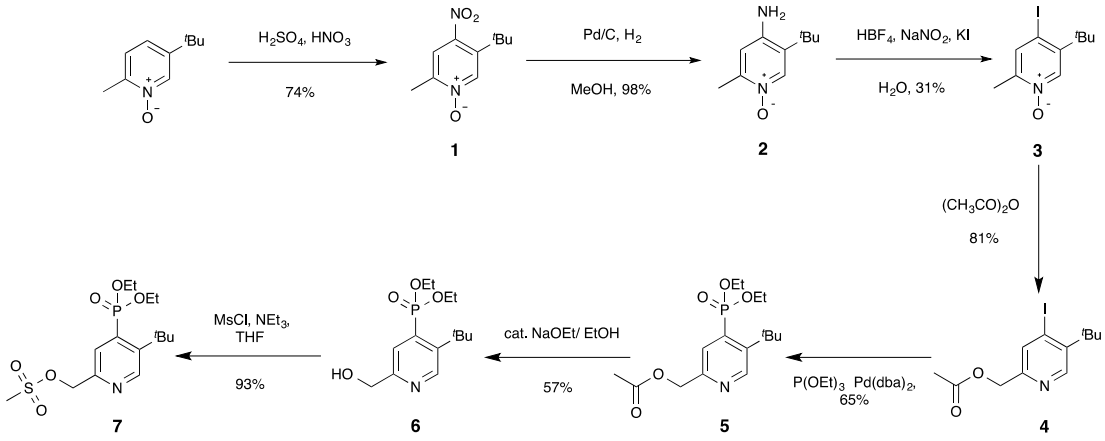

Scheme 2

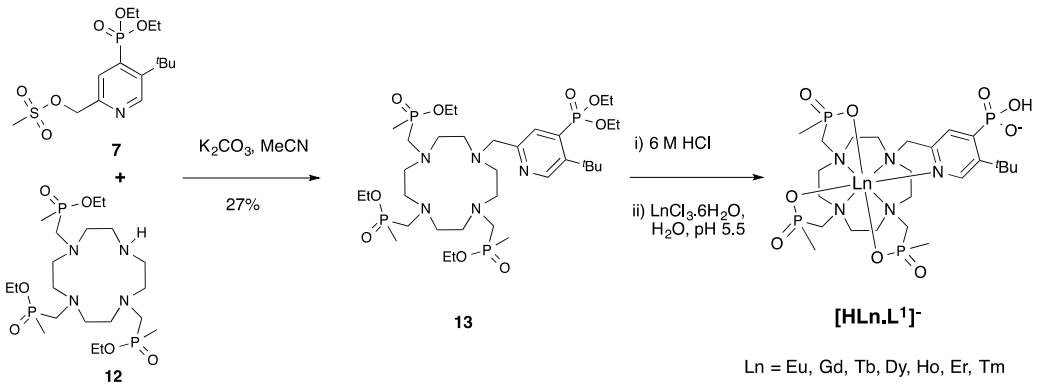

Scheme 3

The triester, **12** (ESI for synthesis) was prepared from mono-BOC-cyclen, and alkylation with **7** in acetonitrile yielded the penta-ester, **13**, which was hydrolysed under acidic conditions. Complexes with seven different lanthanide ion salts were prepared, $[HLn.L^1]^-$, (Ln = Eu, Gd, Tb, Dy, Ho, Er and Tm), each of which was purified by reverse phase HPLC.

Temperature and pH Dependence of the Chemical Shift

Chemical shift data for the paramagnetic complexes (Table 1) shows the very large chemical shift range for the *t*-butyl resonance: from +74 ppm for the thulium complex to -78 and -83 ppm for the Dy and Tb complexes respectively. The unusually large shifts for the Tm and Tb complexes do *not* follow the expected trend predicted by Bleaney's theory of magnetic anisotropy. Such behaviour is in agreement with recent observations that have highlighted the need to appreciate that this theory is *not* generally applicable, and is quite imprecise when the relative magnitude of the components of the magnetic susceptibility tensor varies from one lanthanide to another, within a common isostructural series. [7,17]

The chemical shift of the ^{t}Bu group varied as a function of pH, (Figure 1) allowing pK_a values to be determined, associated with protonation of the phosphonate group. Two major isomeric species were observed in a 5:1 ratio that was more or less invariant with the nature of the lanthanide ion. The minor species was shifted to higher frequency by *ca*. 2.5 ppm across the pH range. Previous work with the parent complex lacking the phosphonate group and its analogues has suggested that the major species observed in solution derives from the enantiomeric (*RRR*-Λ–$\lambda\lambda\lambda\lambda$) and (*SSS*-$\Delta$–$\delta\delta\delta\delta$) complexes, in which the lanthanide ion is 8-coordinate and adopts a twisted square anti-prismatic structure. [8] The minor isomer, by analogy with the stereoisomerism found for related mono-substituted triphosphinates [18a] is most likely to be the enantiomeric pair, (*SSS*-Λ–$\lambda\lambda\lambda\lambda$) and (*RRR*-$\Delta$–$\delta\delta\delta\delta$), as suggested by recent studies, in which X-ray and NMR structural analysis of an analogous Yb complex,

lacking the 4-phosphonate substituent, has confirmed the Yb(III) ion to be 8-coordinate, in a twisted square-antiprismatic geometry with an *RRR-Λ–(λλλλ)* configuration. [18b]

Table 1 ^{1}H NMR shift data for the ^{t}Bu reporter resonance in $[HLn.L^{1}]^{-}$ (295 K, D_2O)

Ln	δH^{a} /ppm	range of pH sensitivity /ppm	T sensitivity ppm/K	p*K*a [b] (error)
Tb	–84.1	1.4	+0.52	7.20(05)
Dy	–79.1	1.9	+0.41	7.11(04)
Ho	–33.0	1.1	+0.17	7.12(04)
Er	+42.2	0.7	–0.24	7.11(04)
Tm	+74.8	1.1	–0.44	7.26(05)

[a] Maximal chemical shift where pD < 5.5; pD values were estimated using the equation: pD = pH (meter reading) + 0.41.

[b] The reported error in the stated pK_a value reflects the goodness of the statistical fit; for pK_a values in serum and in 0.1 M NaCl, see Figures 3 and 4 : a pH titration in 50:50 murine plasma/H_2O for $[HDy.L^{1}]$ gave a pK_a value of 6.80 (±0.08) (295 K).

The pK_a values averaged 7.16(±0.06) in D_2O, in agreement with values expected for ionization of phenylphosphonic acid, [12] suggesting that the ^{t}Bu group does not impose any steric effect to inhibit hydration of the anionic species involved in the equilibrium. In 0.1 M NaCl, the pK_a reduced to 6.71(06), in accord with the expected ionic strength dependence for phosphonate ionization (Figure 2). Surprisingly but usefully, the shift range of pH sensitivity varied from one lanthanide complex to another, (Figure 3), yet not in a manner that was consistently proportional to the size of the pseudo-contact shift.

In contrast, the pseudo-contact shift inherently exhibits a precise T^{-2} dependence on absolute temperature that approximates well to T^{-1} over the physiological temperature range (Table 1, Figures 4 and 5), and was observed to be independent of pH and solvent composition. Thus, given that the Tm and Dy complexes show different pH/shift and temperature dependencies, the observed shifts for each complex in the region of interest being examined *in vivo*, at a given pH and *T*, allow both the *T* and the pH to be calculated when each complex is observed simultaneously using spectroscopic imaging, with a ‘triple imaging’ pulse sequence.

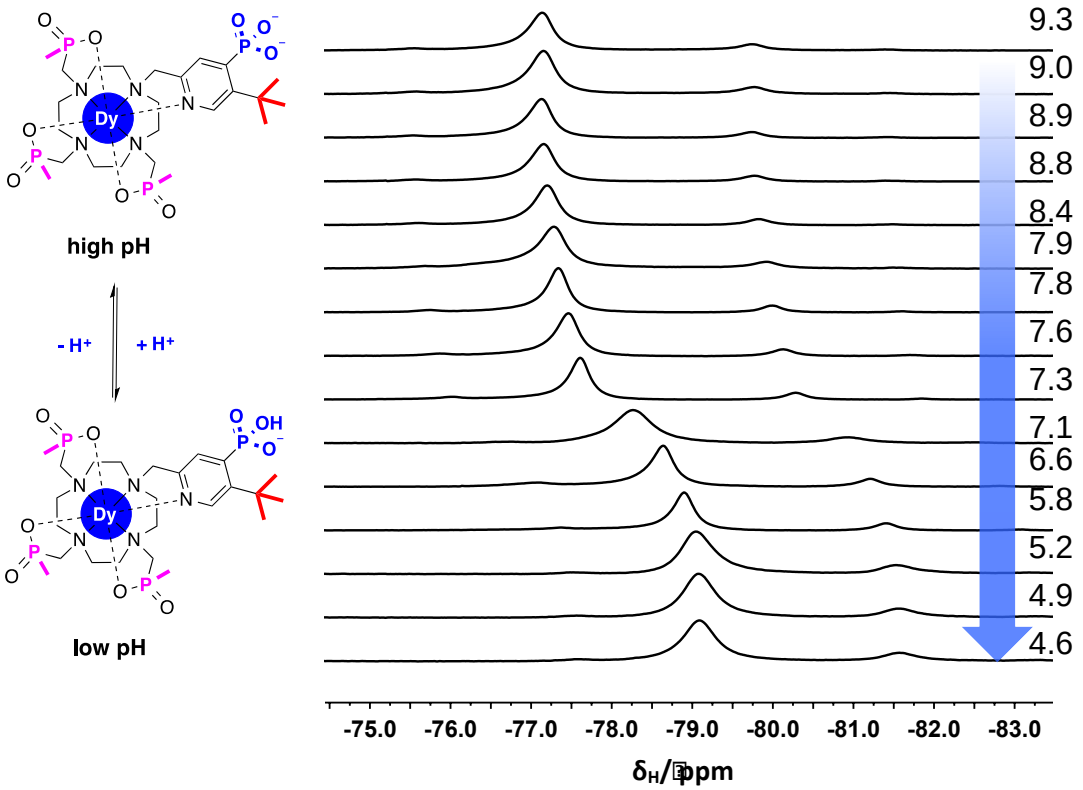

Figure 1. The shift in the major *tert*-butyl resonance of **[Dy.L^1]** as a function of pD (D_2O, 11.7 T, 295 K) and the corresponding protonation equilibrium.

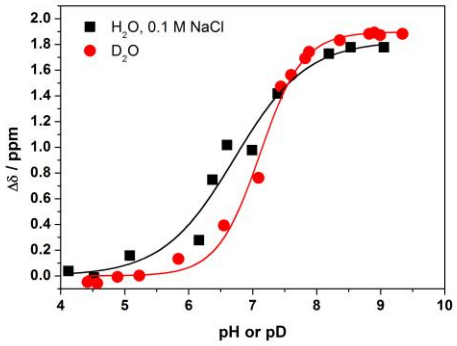

Figure 2. The shift in the major *tert*-butyl resonance of **[Dy.L^1]** as a function of pH or pD in an 0.1 M NaCl solution in H_2O (*black*), pK_a = 6.71(0.06), and in pure D_2O (*red*), pK_a = 7.11(05) (11.7 T, 295 K).

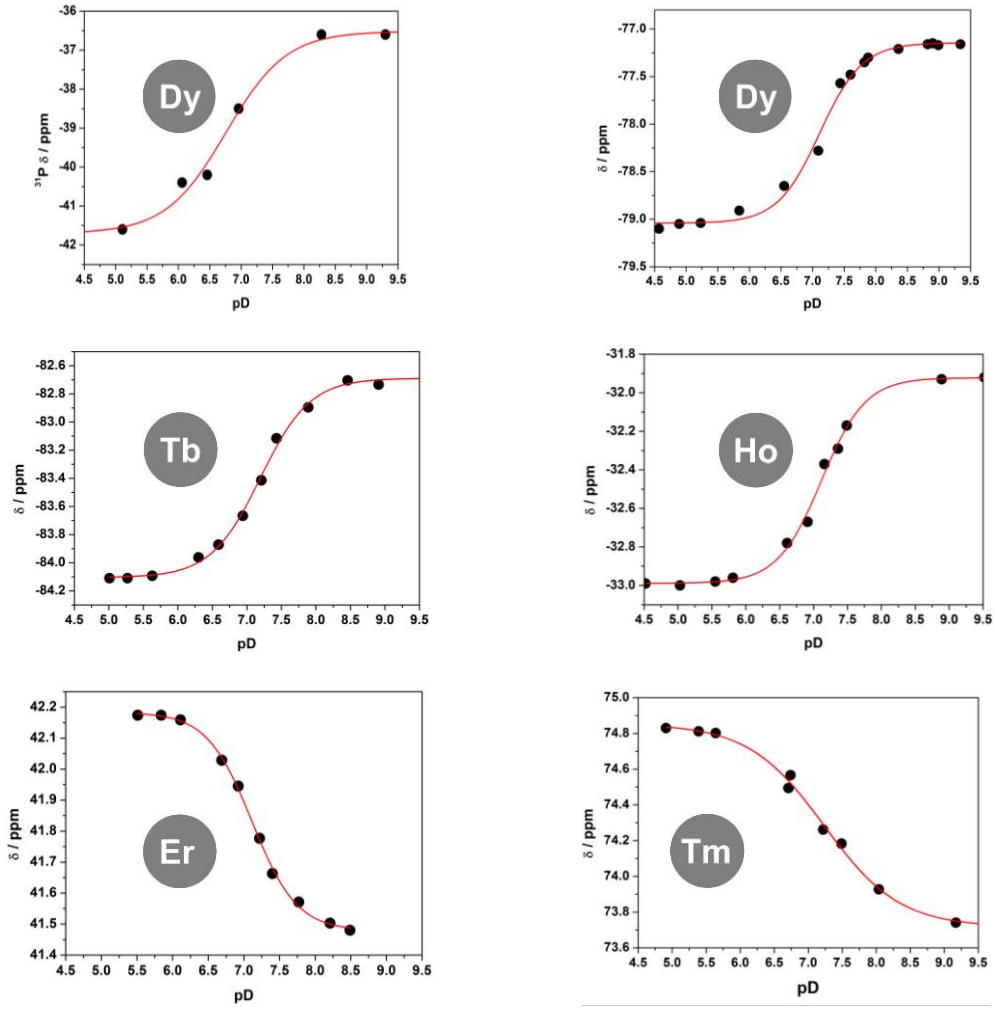

Figure 3. (*upper left*) Variation in the ^{31}P phosphonate shift for **[HDy.L^{1}]$^{-}$**; (*remainder*): variation of the ^{1}H NMR shift for the major *tert*-butyl resonance of **[HLn.L^{1}]$^{-}$** (Ln = Dy, Tb, Ho, Er and Tm) as a function of pD (D_2O, 11.7 T, 295 K: see Table 1 for pK_a data).
A pH titration in a 50:50 mixture of murine plasma/H_2O also gave rise to a +1.8 ppm shift in the tert-butyl resonance, with a pK_a of 6.80 (±0.08) (11.7 T, 295 K), suggesting that the presence of protein has relatively little effect on the protonation equilibrium.

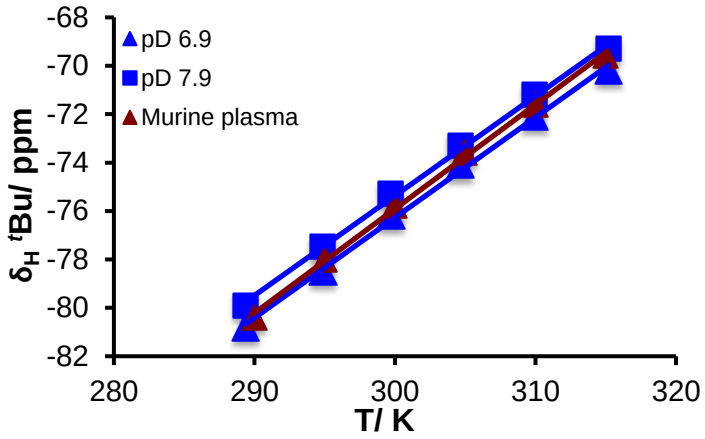

Figure 4. Variation in the chemical shift of the major *tert*-butyl resonance of **[Dy.L^1]$^-$** as a function of T: pD 6.9 (blue triangles), gradient = 0.414, R^2 = 0.998; pD 7.9 (blue squares), gradient = 0.414, R^2 = 0.998; and in a 50:50 murine plasma: H_2O mix at pH 7.1 (red triangles), gradient = 0.431, R^2 = 0.999 (11.7 T).

Field dependence of relaxation rate measurements

Earlier, we and others have shown that the occurrence of fast relaxation allows shorter acquisition times to be used in gradient echo and related pulse sequences, leading to increases in signal intensity per unit time of the order of 15 to 25 times, versus a diamagnetic control. [4-6] The longitudinal relaxation rate, R_1, of each complex was measured at six fields over the range 1 to 16.5 Tesla. Relaxation rates were fastest at 1T for the erbium and dysprosium complexes, and values were broadly similar in the field range 4.7 to 9.4 T (Table 2). Such behaviour reflects the additive contributions of dipolar and Curie contributions to relaxation, which are hypothesized to have squared and fourth power dependences on the mean magnetic susceptibility, in the most commonly used model used to treat paramagnetic relaxation, based on Bloch-Redfield-Wangsness theory, eq 1. [19]

$$R_1 = \frac{2}{15}\left(\frac{\mu_0}{4\pi}\right)^2 \frac{\gamma_N^2 \mu_{eff}^2}{r^6}\left[\frac{7\tau_{R+e}}{1+\omega_e^2\tau_{R+e}^2} + \frac{3\tau_{R+e}}{1+\omega_N^2\tau_{R+e}^2}\right] + \frac{2}{5}\left(\frac{\mu_0}{4\pi}\right)^2 \frac{\omega_N^2 \mu_{eff}^4}{(3kT)^2 r^6} \frac{3\tau_R}{1+\omega_N^2\tau_R^2} \qquad (1)$$

$$\mu_{eff}^2 = g_e^2 \mu_B^2 \left\langle \hat{S}^2 \right\rangle \qquad \tau_{R+e} = \left(\tau_R^{-1} + T_{1e}^{-1}\right)^{-1}$$

where μ_0 is the vacuum permeability, g_N is the gyromagnetic ratio of the nucleus, g_{Ln} is the Landé factor of the fundamental multiplet J of the free Ln^{3+} ion, τ_r is the rotational correlation time in which isotropic tumbling is assumed, μ_B is the Bohr magneton (BM), r is the electron-nuclear distance, ω_N is the nuclear Larmor frequency, ω_e is the electron Larmor frequency and T_{1e} is the longitudinal relaxation time of the electron spin. In this approximation, at low magnetic fields, relaxation is dominated by electronic relaxation (T_{1e}), while at higher fields the order of relaxation tends to echo the size of the magnetic susceptibility, μ_{eff}. Relaxation

rates were found to vary by less than 2 to 3 % as the pH was varied over the studied range (11.7 T, 310K).

Global minimisation methods were applied to the 5 data sets together and assuming classical BRW theory (eq. 1), values of μ_{eff} , τ_r and T_{1e} were estimated (Table 3 and Figure 5). The Ln-^{t}Bu hydrogen average distance, was assumed to be 6.6 Å, neglecting the minor variation of ionic radius associated with the lanthanide contraction (0.07 Å from Tb to Tm). The value of *r* has been shown earlier to correspond to the average distance estimated using DFT calculations, based on consideration of closely related X-ray structural analyses. [8] A global minimum was found, with τ_r = 341 (9) ps, and the best-fit values of T_{1e} and of μ_{eff} are given below (Table 3). The highest value of T_{1e} was found for erbium, in accord with its unique low field relaxation behaviour. Furthermore, values of μ_{eff} deviated significantly from the commonly accepted free-ion values, notably for Er (+15%) and Tm (+37%), (Table 3), which fitted least well (Figure 5). It has been suggested that such behaviour reflects the inadequacy of this theoretical model, [17] and relaxation needs to consider the anisotropy of the magnetic susceptibility tensor explicitly, in a modified approach first suggested by Fiat and Vega. [20] The fast and similar relaxation rates of the Tm and Dy complexes in the field range 4.7 to 11.7 T, coupled with their large shift and most favourable pH/*T* dependencies , encouraged the assessment of the utility of this pair of complexes for multiple imaging studies.

Table 2. ^{1}H NMR longitudinal relaxation rate data for $[Ln.L^1]^{2-}$ (295 K, D_2O, pD 7.4) as a function of magnetic field (Tesla) .[a,b]

	$R_1(s^{-1})$					
Ln	1 T	4.7 T	9.4 T	11.7 T	14.1 T	16.5 T
Tb	42(3)	73(1)	122(2)	134(1)	150(1)	164(1)
Dy	54(5)	88(3)	156(1)	179(1)	195(1)	218(1)
Ho	44(4)	89(5)	160(2)	191(2)	209(1)	252(1)
Er	92(10)	117(7)	173(3)	198(3)	214(7)	239(8)
Tm	25(4)	81(4)	139(1)	160(1)	179(1)	194(1)

[a] At 9.4 T and pD 9, the ratios of R_1/R_2 were: Tb, 0.30; Dy, 0.50; Ho, 0.46; Er, 0.38; Tm, 0.58; at the pK_a, the ratio was 0.20, reflecting the impact of chemical exchange (uncertainty) broadening.

[b] Errors are given in parenthesis.

Table 3. Estimated 'best fit' values for ^{1}H NMR relaxation parameters following global fitting with r = 6.6 Å [a,b] (295 K, D_2O, data in Table 2 ; fits in Figure 5) for $[Ln.L^1]^{2-}$

Ln	T_{1e}/ps	μ_{eff}/BM
Tb	0.44(3)	9.89(2)
Dy	0.46(5)	10.65(2)
Ho	0.34(5)	10.99(2)
Er	0.79(9)	10.80(4)
Tm	0.30(4)	10.46(3)

[a] The five data sets were fitted globally, using r = 6.6 Å, where r is the mean distance between the lanthanide ion and the ^{t}Bu hydrogen atoms, data minimised to give τ_r = 345(7) ps; [b] classical values for the magnetic moments of lanthanide(III) ions are: Tb, 9.8; Dy, 10.3; Ho, 10.4; Er, 9.4; Tm, 7.6 BM.

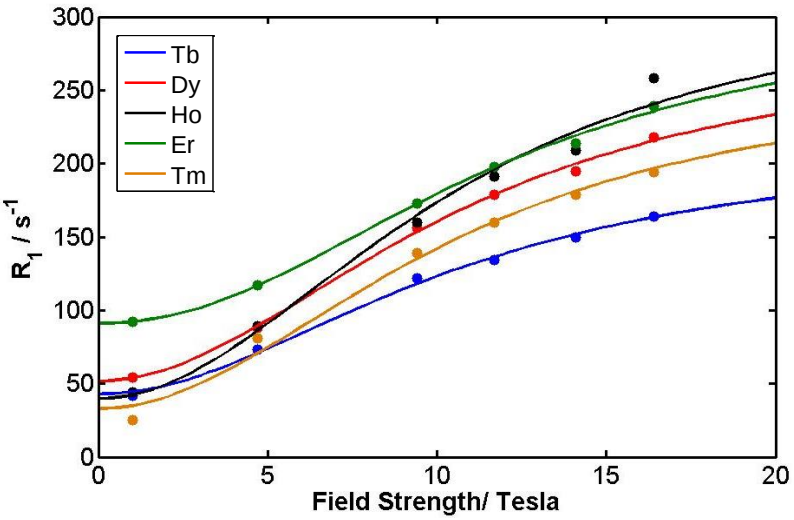

Figure 5. ^{1}H NMR relaxation rates (R_1/s^{-1}) for the ^{t}Bu resonance in $[Ln.L^1]^{2-}$ as a function of magnetic field, showing the global fits (line) to the experimental data points (295K D_2O, pD 7.4, fixed r = 6.6 Å, minimizes to τ_r = 345(9) ps)

Phantom and *in vivo* imaging and shift imaging studies

Phantom imaging studies at 300 MHz (7 T) were undertaken to assess the feasibility of imaging at these very well separated spectral frequencies. Equimolar solutions of both $[Dy.HL^1]^-$ and $[Tm.HL^1]^-$ (ESI) were prepared in buffered aqueous solution (0.1 M MOPS), at a range of pH values, inside cut-down 5 mm NMR tubes. The NMR tubes were placed within a Teflon spacer, (Figure 6) with an NMR tube containing only de-ionised water, occupying the central position. The experimental array was placed inside the bore of a 30 mm birdcage coil, typically used for murine imaging. First, an image corresponding to the water protons

was obtained by imaging with a 3-dimensional gradient echo (3D-GE) MR sequence at the H_2O offset. Second, 3DGE images of the *tert*-butyl reporter resonances were acquired by setting the excitation offset to the resonant frequency of the ^{t}Bu resonance in each lanthanide complex at pH 7. The combination of the large offset frequency with selection of a narrow (20KHz) spectral bandwidth allowed, the *tert*-butyl reporter resonance to be acquired, separately from the water signal.

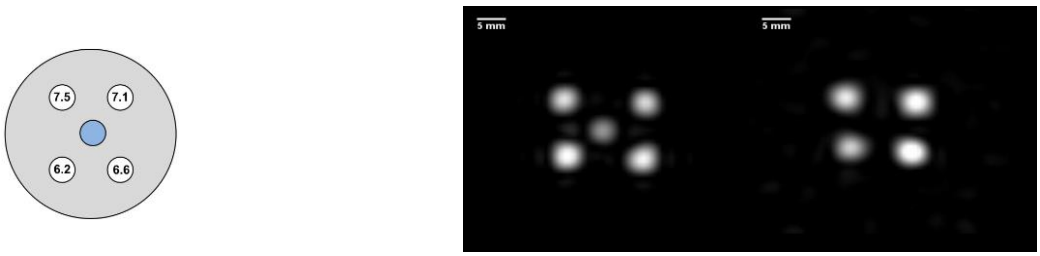

Figure 6. (*Left*) Illustration of experimental array, in a Teflon holder, using 4 equimolar solutions of buffered **[Dy.HL^1]$^-$** at different pH values shown and with de-ionised water in the centre (MOPS, 1.2 mM, H_2O). (*Middle*) Phantom image at the H_2O offset (intensity scale 0-4000 a.u.). (*Right*) Phantom image at the **[Dy.HL^1]$^-$** *tert*-butyl offset (-23474 Hz, intensity scale 0-0.1 a.u.), both: TR/TE=17.2/0.7 ms; averages 4 (H_2O), 30 (*tert*-butyl); spectral width, SW = 8103 Hz; spectral points = 128; matrix 16 x 16; FOV 40 x 40 mm; slice thickness = 4 mm; T = 310 K).

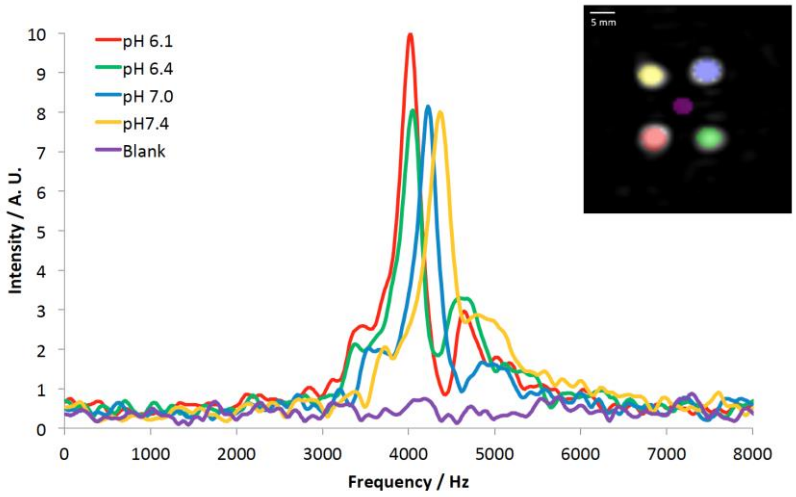

Figure 7. Spectral analysis from the spectroscopic imaging study of **[Dy.HL^1]$^-$**, showing the frequency detected for each ROI peak for: pH 6.2 (red), 3543 Hz; 6.6 (green), 3644 Hz; 7.1 (blue), 3773 Hz; and 7.5 (yellow), 3861 Hz. Total shift = 318 Hz = 1.06 ppm; offset frequency = -23474 Hz. TR/TE = 17.2/0.7 ms, 30 averages, slice thickness = 60 mm, 128 spectral points, SW = 8013 Hz, T = 310K.

Spectroscopic images were then collected using a 2DSI sequence. This method selected a single imaging slice through the phantom and encoded the spatial location of the signal to

provide a complete NMR spectrum at each point in the image matrix, allowing spectral analysis of resonance frequency as a function of pH for each tube of the experimental phantom (Figure 7). With a total shift of 318 Hz at 7 T (1.06 ppm) between pH 6.2 and 7.5, the data obtained was in good agreement with results found *in vitro*, (Table 1). The pH dependent shift for **[**Dy.HL]$^{-}$ was greater over this range than for [Tm.HL^{1}]$^{-}$ (1.06 ppm *vs.* 0.48 ppm). The difference in the size of the shift change is somewhat surprising, but is very useful, as it distinguishes each from the accompanying temperature dependent behaviour, where the large positive (Tm) or negative (Dy) paramagnetic shift diminishes as temperature increases.

The temperature of five solutions of [Tm.HL^{1}]$^{-}$ used in the phantom studies was varied, using an externally controlled heated airflow around the Teflon spacer array, and was monitored by positioning a MRI compatible thermometer in the middle of the array. Spectroscopic images were acquired 5 minutes after setting the temperature, in order to minimise any chemical shift fluctuations, (Figure 8).

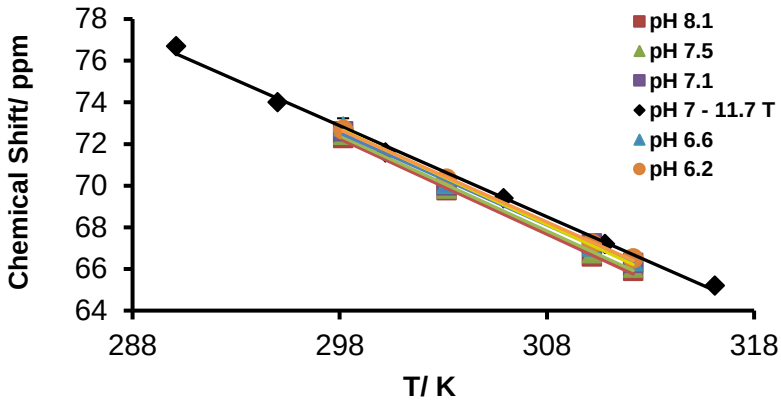

Figure 8. Variation in the chemical shift of the major *tert*-butyl resonance of five different pH solutions of [Tm.HL^{1}] as a function of temperature (7 T): pH 6.2 (orange), gradient = -0.44; pH 6.6 (blue), gradient = -0.46; pH 7 (black), gradient = -0.44; pH 7.1 (purple), gradient = -0.44; pH 7.5 (green), gradient = 0.46; and pH 8.1 (red), gradient = -0.46. Each line of best-fit has R^2 = 0.998.

The *tert*-butyl chemical shift of each of the five solutions measured from the spectroscopic imaging data revealed a linear temperature dependence over the range examined, with the variation in agreement with data obtained in NMR spectroscopy experiments at 11.7 T at pH 7. In each case, the *tert*-butyl group gave rise to a chemical shift temperature dependence of -0.45±0.01 ppm/K. With [Dy.HL^{1}]$^{-}$ the temperature dependence was found to be +0.41±0.01 ppm/K.

Preliminary Triple Imaging Phantom and In Vivo Studies

Phantom triple imaging studies were next undertaken using a solution containing equimolar concentrations of both the Dy and Tm complexes (1.2mM each [Ln.HL[1]], 0.1 M NaCl, 310K). A pulse sequence was developed to enable triple imaging, which allows simultaneous signal acquisition from all 3 signal sources - the normal tissue water signal and each of the well-separated *t*-butyl signals. This pulse sequence used a dual, back-to-back RF pulse to consecutively excite the Dy and Tm complexes. The frequency, shape, duration and power of both excitation pulses could be separately modified. Fortunately, the relaxation times (T_1 and T_2) of each complex have the same values, within experimental error, at 7 Tesla (T_2 and T_1 = 3.4 and 7.8 ms) and so the same shape, duration and power could be used for each complex, and it was only necessary to change the offset frequency. The encoding gradients were then applied, and the spectral width (SW) was increased to ~60 kHz, in order to encompass signal from all three frequency ranges. No explicit excitation pulse was applied to the water resonance frequency, as there was sufficient excitation within the bandwidth of the main RF pulses. The dual RF pulse train was applied to both a spectral imaging pulse sequence and a 3D-gradient echo pulse sequence (Figure 9).

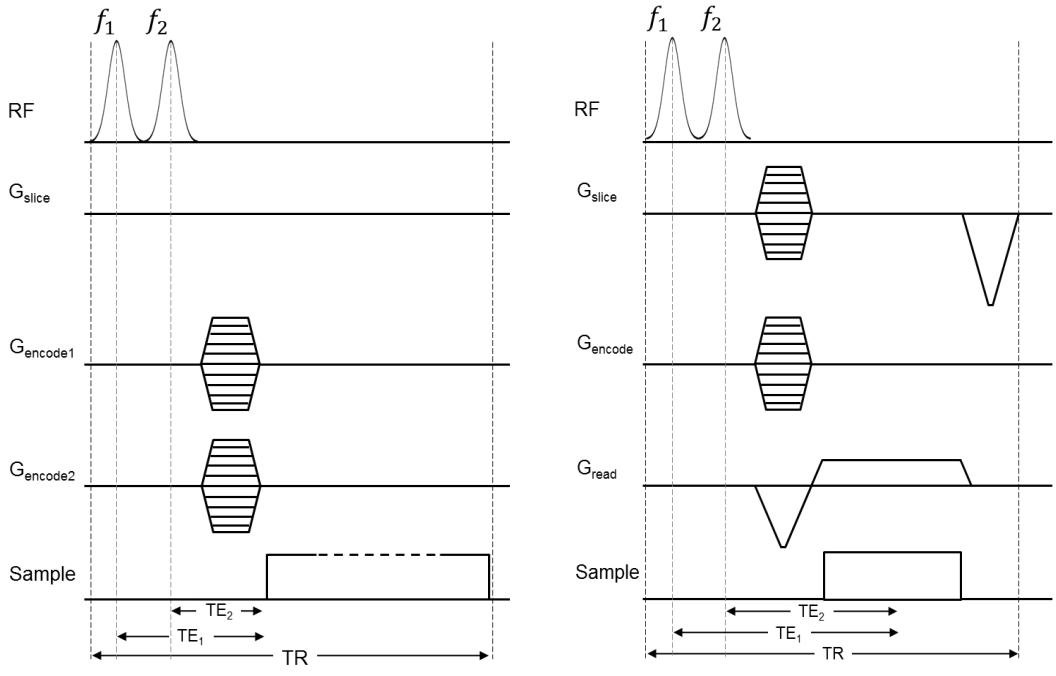

(a) 2DSI (b) GE3D

Figure 9. Pulse sequence diagrams for: (a) a spectral imaging (2DSI) pulse sequence and, (b) a 3D-gradient echo pulse sequence where f1 and f2 are 'back to back', Gaussian shaped excitation pulses applied at the respective transmit frequencies of the *tert*-butyl resonances (frequencies f1 and f2), each with a duration of 500 μs.

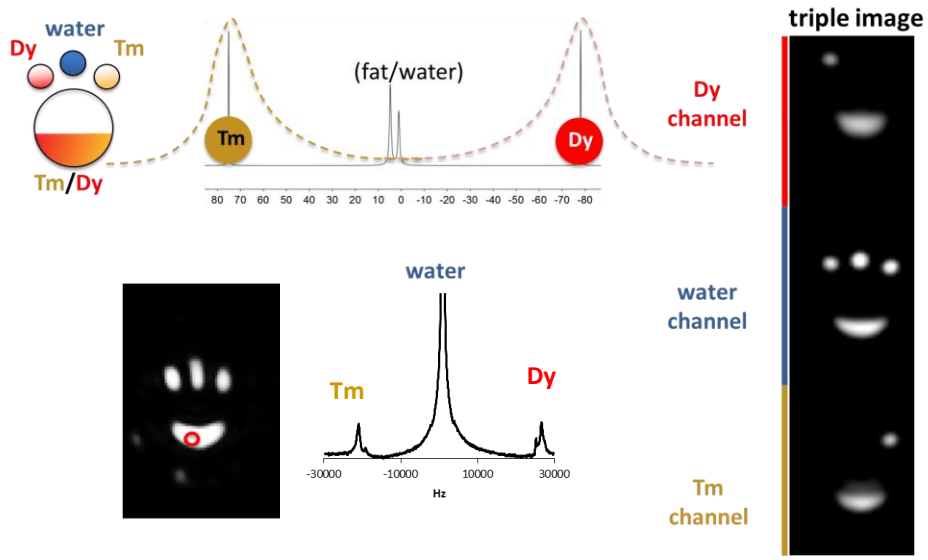

Figure 10. *Left*: a spectral imaging sequence applied to a phantom set-up, with a TR of 19.5 ms, TE_1 of 0.95 ms TE_2 of 0.45 ms and a spectral width SW of 54 kHz, 32 averages, scan time = 100 s. *Right*: a 3D-gradient echo pulse sequence with a TR of 4.28 ms, TE_1 (Dy) of 0.87 ms, TE_2 (Tm) of 1.37 ms, SW = 60 kHz, 80 averages, scan time = 354 s. The phantom contained NMR tubes containing 1.2 mM [Tm.HL[1]], [Dy.HL[1]] or water and a small vial containing equimolar mix of the two complexes.

Figure 10 illustrates the *in vitro* 3DGE and 2DSI results. Using the 3DGE approach with a triple imaging bandwidth (and triple number of sample points) relative to a normal MRI acquisition allows sampling across the full MRI frequency range arising from the water, Tm and Dy agents. The right panel illustrates the full triple imaging field of view which can be split into 3 entirely independent MRI images of the Dy, water and Tm. The lower vial of the phantom contains aqueous solutions of a mixture of the Dy and Tm complexes appears in each of the channels. The central small tube containing only water appears in the central water image and the other tubes containing only Dy or only Tm appear in their respective channels. This approach does not degrade the signal to noise ratio of the scan relative to acquiring individual images of each component with separate excitations, as the noise bandwidth per pixel is unchanged. The MRSI acquisition generates a matrix of voxels, each of which can be interrogated to show the full spectral range. Individual peaks from water, and the Tm and Dy complexes are clearly observed as expected in the example voxel from the mixed solutions in the lower vial.

These sequences were applied *in vivo* following tail-vein injection of CD1 healthy mice *(n=3)* with 0.05 mmoles/kg of a 1:1 mixture of the Tm/Dy complexes in saline. Illustrative data from one mouse are shown (Figure 11), where data were collected with the MRSI sequence to follow the kinetics of the complex through the tissue. Selected spectra from the MRSI data

grid were extracted to illustrate the large shifts seen in the high and low frequency regions of the spectrum (Figure 11, stacked spectra), and clearly demonstrate changes in frequency between tissues, most markedly in the bladder, with the shifts attributable to differences in tissue pH and temperature. A 3DGE acquisition was also acquired (Figure 11, right). The central region of the triple image shows the standard water (and fat) MRI, but at the time this image was taken, 40 minutes post injection, renal clearance of the contrast agent resulted in a strong signal from the bladder only.

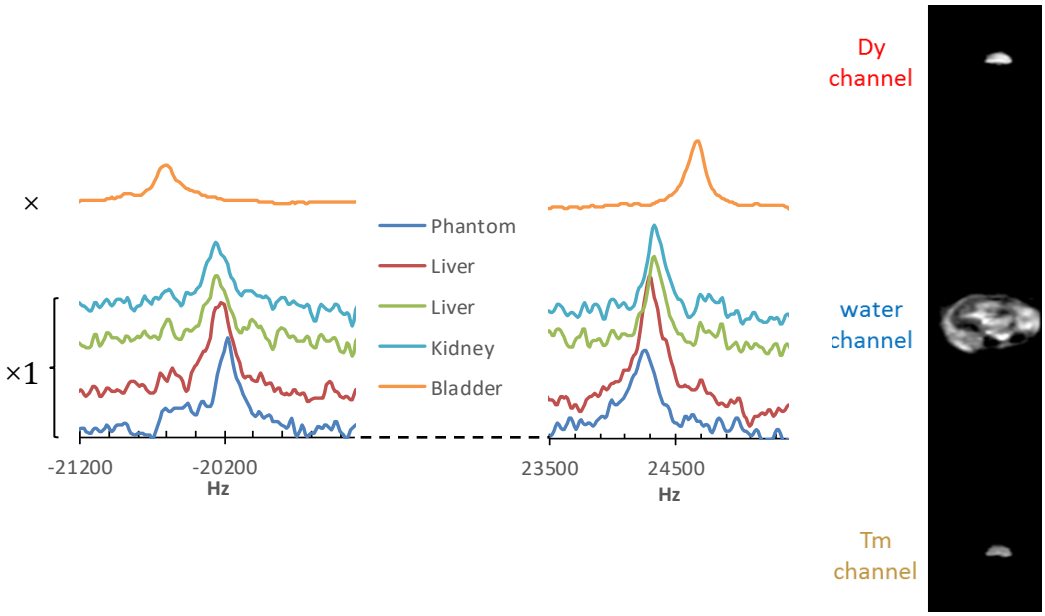

Figure 11. In vivo examples of 3DGE and MRSI acquisition in an intact, healthy mouse following single i.v. injection of a mix of Dy and Tm PARASHIFT contrast agent. *Left* : Selected spectra from a time series of 2DSI acquisitions. The stacked spectra ,where the y axis denotes signal intensity in arbitrary units, show the Tm (left) and Dy (right) spectral regions from voxels sampling liver (two time points), kidney, bladder and an external reference phantom. MRSI acquisition parameters were TR 19.5 ms, TE_1 (Dy) 0.45 ms, TE_2 (Tm) of 0.95 ms, SW 54 kHz, 32 averages, scan time 100 s. *Right* : a 3DGE triple image using a pulse sequence with TR of 10.66 ms, TE_1 of 1.58 ms, TE_2 of 2.08 ms, SW = 54 kHz, 100 averages, scan time = 1092 s.

The frequency shift of each resonance was measured in these spectra by peak picking and the pH and temperature determined by solving the simultaneous equations defining the frequency versus pH and T dependence for each complex (see ESI). Liver pH was measured to be 7.14, kidney pH was 6.92 and bladder pH was 6.8, consistent with the expected range of values for normal wild type animals. Temperature was also significantly lower in the bladder (3.5 C below core body temperature) and this temperature difference is the cause of the large frequency shift in the bladder resonances, relative to the other tissues. With the aid of zero-filling of the raw spectra, (see SI for a discussion) the accuracy of spectral frequency measurement for in vivo 2DSI acquisitions was assessed as being 13 Hz, which is equivalent to a temperature accuracy of ±0.1C.

The accuracy of pH measurement is non-linear given the sigmoidal relationship between frequency and pH, being greatest (±0.1 pH units) around pH 7.2 (see ESI). The pH accuracy of our measurements are similar to recent attempts to measure tissue pH using indirect detection of contrast agent (iopamidol) presence using chemical exchange saturation transfer (CEST) methods [11d], which also suggests an accuracy of ±0.1 pH units, but which is dependent on concentration. Those CEST methods have been attempted in human subjects to measure bladder pH and in animal models and human subjects to measure tumour pH [11f] In those studies the authors note the sensitivity of their methods to experimental parameters (such as the B_1 field of the CEST saturation) and choice of modelling approaches, which are consequences of the indirect detection use for CEST imaging, but which are absent from the PARASHIFT method using the frequency shift of the directly detected complex. Further challenges were noted due to rapid clearance of the complex which is a common problem for all molecular MRI tracer experiments.

Other studies using similar paramagnetically shifted resonance detection to measure tissue pH in rats have demonstrated elegant pH maps with good spatial resolution through the use of renal ligation or pharmacological manipulation of renal excretion combined with long, steady infusion rates of several hours [15]. In this study, we have constrained our *in vivo* work to use a single i.v. bolus of complexes at a clinically equivalent dose level and to follow this in intact mice with no modification of renal excretion rates. The data demonstrate that this approach is feasible with these complexes, but the approach necessarily limits the achievable resolution due to the short scan durations used.

Summary and Conclusions

The Dy and Tm complexes of L^1 have several key properties that favour their simultaneous observation, together with the water signal, in triple imaging experiments at 7 T. They exist in aqueous solution as one major stereoisomer; thus, one main signal is observed for the *t*-butyl ^{1}H NMR reporter group that resonates over 70 ppm from the water signal. Furthermore, they possess R_1 and R_2 values that are within 10% of each other, so that Ernst angle pulsing conditions which achieve optimum imaging sensitivity are achieved using the same shape, duration and power of each excitation pulse in gradient echo 3D Imaging and 2D spectral imaging experiments; only the offset frequency needed to be changed. Under the conditions used, the intense water signal was co-observed without the need for separate excitation. The shifted *t*-butyl signals exhibit a large dependence on temperature, +0.41 and -0.44 ppm for the Dy and Tm complexes respectively. Protonation of the aryl phosphonate group leads to a shift of +1.9 ppm, $[Dy.L^1]^{2-}$ and -1.1 ppm for $[Tm.L^1]^{2-}$; even at a pH corresponding to the pK_a value, uncertainty broadening due to chemical exchange means that the R_1/R_2 ratio was not less than 0.2, and so did not inhibit spectral or image acquisition unduly.

The dual temperature and pH sensitivity of the reporter chemical shift means that both complexes need to be present in the region of interest examined, in order to observe two shift values, the simultaneous equation of which can be solved for T and pH. In this manner, using appropriate phantoms to provide the calibration values, the pH and temperature of the liver was assessed to be 7.1 and 34.5°C, whilst the values for the bladder were 6.8 and 31°C.

These approaches allow simultaneous spectroscopic imaging of pH and T, and with appropriate post-processing can be used to generate pH and T maps, for the liver and kidneys in particular, that may be of benefit to radiologists seeking to identify areas of inflammation and fibrosis where elevated temperature, for example, may occur.

Experimental

Details of NMR data acquisition, relaxation measurements and analysis, and the estimation of T and pH in PARASHIFT experiments are given in the supplementary information.

Ligand and complex synthesis

5-*tert*-Butyl-2-methyl-4-nitropyridin-1-oxide

5-*tert*-Butyl-2-methylpyridine 1-oxide (3.20 g, 19.4 mmol) was dissolved in conc. H_2SO_4 (98%, 11.0 mL, 209.5 mmol) and stirred for 10 min at 5 °C. To this solution was added HNO_3 (70%, 7.0 mL, 161.0 mmol) dropwise and the resulting mixture was heated to 100 °C for 18 h. After this time, the solution was dropped onto ice and stirred for 1 h before the aqueous mixture was extracted with CH_2Cl_2 (3 × 150 mL). The organic layers were combined, dried over $MgSO_4$ and the solvent removed under reduced pressure. The resulting pale green oil was purified by silica gel column chromatography, eluting with a gradient starting from 100% CH_2Cl_2 to 2% MeOH/ CH_2Cl_2, to yield a bright yellow oil (3.0 g, 74%). R_f (10% MeOH/ CH_2Cl_2) = 0.47; ^{1}H NMR (400 MHz, $CDCl_3$) δ 8.76 (s, 1H, H^6), 7.58 (s, 1H, H^3), 2.64 (s, 3H, CH_3), 1.35 (s, 9H, $C(CH_3)_3$); ^{13}C NMR (101 MHz, $CDCl_3$) δ 152.5 (C^2), 151.1 (C^5), 142.3 (C^6), 139.3 (C^4), 122.6 (C^3), 35.7 ($\underline{C}(CH_3)_3$), 29.9 ($C(\underline{C}H_3)_3$), 17.5 (CH_3); ESI-LRMS (+)

m/z 211.1 $[M+H]^+$; ESI-HRMS (+) calcd for $[C_{10}H_{15}N_2O_3]^+$ 211.1083, found 211.1088.

4-Amino-5-*tert*-butyl-2-methylpyridin-1-oxide

5-*tert*-Butyl-2-methyl-4-nitropyridin-1-oxide (1.9 g, 9.04 mmol) was dissolved in MeOH (50 mL) and Pd/C was added (Pd content 10 %, 190 mg). The vessel was then loaded onto a Parr hydrogenator (pressure 40 bar H_2) and the reaction mixture was agitated for 18 h. After this time, the mixture was filtered before the solvent was evaporated under reduced pressure to yield an orange oil (1.6 g, 98%). R_f (10% MeOH/ CH_2Cl_2) = 0.28; ^{1}H NMR (400 MHz, CD_3OD) δ 7.95 (s, 1H, H^6), 6.68 (s, 1H, H^3), 3.32 (s, 3H, CH_3), 1.37 (s, 9H, $C(CH_3)_3$); ^{13}C NMR (101 MHz, CD_3OD) δ 152.2 (C^2), 148.0 (C^5), 138.1 (C^6), 129.4 (C^4), 112.2 (C^3), 34.1 ($\underline{C}(CH_3)_3$), 26.8 ($C(\underline{C}H_3)_3$), 16.9 (CH_3); ESI-LRMS (+) *m/z* 181.1 $[M+H]^+$; ESI-HRMS (+) calcd for $[C_{10}H_{17}N_2O]^+$ 181.1341, found 181.1350.

5-*tert*-Butyl-4-iodo-2-methylpyridin-1-oxide

To a cold solution of 4-amino-5-*tert*-butyl-2-methylpyridin-1-oxide (1.6 g, 8.88 mmol) and HBF_4 (2.3 mL, 17.8 mmol) in H_2O (40 mL) was added dropwise, a solution of $NaNO_2$ (1.2 g, 17.8 mmol) in H_2O (5 mL). Potassium iodide (2.0 g, 12.4 mmol) was slowly added to the suspension, in several portions. The reaction mixture was allowed to stir at rt for 5 min before being heated at 60 °C for 30 min. The mixture was cooled to rt and the pH adjusted to 10 with KOH. The solution was extracted with CH_2Cl_2 (3 × 100 mL) and washed with $NaHCO_3$ (sat. aq. solution, 100 mL) before being dried over $MgSO_4$ and the solvent removed under reduced pressure. The resulting brown oil was purified by silica gel column chromatography, eluting with a gradient starting from 100% CH_2Cl_2 to 2% MeOH/ CH_2Cl_2 to yield an orange solid (0.8 g, 31%). R_f (10 % MeOH/ CH_2Cl_2) = 0.37; m.p. 153-155 °C; ^{1}H NMR (400 MHz, $CDCl_3$) δ 8.23 (s, 1H, H^6), 7.80 (s, 1H, H^3), 2.41 (s, 3H, CH_3), 1.48 (s, 9H, $C(CH_3)_3$); ^{13}C NMR (101 MHz, $CDCl_3$) δ 152.5 (C^2), 146.5 (C^5), 139.8 (C^6), 138.4 (C^4), 122.2 (C^3), 35.9 ($\underline{C}(CH_3)_3$), 29.1 ($C(\underline{C}H_3)_3$), 16.7 (CH_3); ESI-LRMS (+) *m/z* 291.9 $[M+H]^+$; ESI-HRMS (+) calcd for $[C_{10}H_{15}{}^{127}INO]^+$ 292.0198, found 292.0208; Anal Calcd (%) for $C_{10}H_{15}INO$: C, 41.26; H, 4.85; N, 4.81, found: C, 41.11; H, 4.78; N, 4.79.

(5-*tert*-Butyl-4-iodopyridin-2-yl)methyl acetate

5-*tert*-Butyl-4-iodo-2-methylpyridin-1-oxide (0.8 g, 2.75 mmol) was dissolved in acetic anhydride (10 mL) and the solution was heated to 75 °C for 3 h. The solvent was removed under reduced pressure and the resulting orange oil was purified by silica gel column chromatography, eluting with a gradient starting from 100% CH_2Cl_2 to 2% MeOH/ CH_2Cl_2 to yield an orange oil (0.74 g, 81%). R_f (10 % MeOH/ CH_2Cl_2) = 0.62; ^{1}H NMR (400 MHz, $CDCl_3$) δ 8.53 (s, 1H, H^6), 7.94 (s, 1H, H^3), 5.11 (s, 2H, CH_2), 2.16 (s, 3H, CH_3), 1.54 (s, 9H, $C(CH_3)_3$); ^{13}C NMR (101 MHz, $CDCl_3$) δ 170.7 (CO), 158.5 (C^2), 147.6 (C^5), 145.0 (C^6), 136.3 (C^4), 107.0 (C^3), 65.5 (CH_2), 35.9 ($\underline{C}(CH_3)_3$), 29.6 ($C(\underline{C}H_3)_3$), 21.0 (CH_3); ESI-LRMS (+) *m/z* 333.8 $[M+H]^+$; ESI-HRMS (+) calcd for $[C_{12}H_{17}{}^{127}INO_2]^+$ 334.0304, found 334.0307.

[5-*tert*-Butyl-4-(diethoxyphosphoryl)pyridin-2-yl]methyl acetate

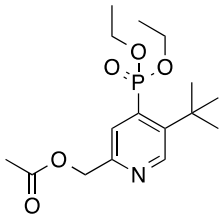

(5-*tert*-Butyl-4-iodopyridin-2-yl)methyl acetate (425 mg, 1.28 mmol) was dissolved in triethylphosphite (10 mL, 58.3 mmol). To this solution was added $Pd(dba)_2$ (73 mg, 10 mol%, 0.128 mmol) and the resulting mixture was heated at 120 °C for 18 h. The solvent was removed by vacuum distillation and the resulting brown oil was purified by silica gel column chromatography, eluting with a gradient starting from 100% CH_2Cl_2 to 1% MeOH/ CH_2Cl_2, to afford a yellow oil (284 mg, 65%). R_f (10% MeOH/ CH_2Cl_2) = 0.56; ^{1}H NMR (400 MHz, $CDCl_3$) δ 8.84 (d, $^4J_{HP}$ = 8, 1H, H^6), 7.80 (d, $^3J_{HP}$ = 16, 1H, H^3), 5.21 (s, 2H, CH_2), 4.05-4.14 (m, $^3J = 7_{HP}$, 4H, $POCH_2$), 2.16 (s, 3H, $pyCH_3$), 1.58 (s, 9H, $C(CH_3)_3$), 1.31-1.37 (m, $^4J = 7_{HP}$, 6H, $POCH_2C\underline{H}_3$); ^{31}P NMR (162 MHz, $CDCl_3$) δ 16.1-16.5 (m, $^3J_{PH}$ = 7); ^{13}C NMR (101 MHz, $CDCl_3$) δ 170.7 (CO), 153.1 (d, $^3J_{CP}$ = 12, C^6), 149.2 (d, $^3J_{CP}$ = 13, C^2), 147.7 (d, $^2J_{CP}$ = 11, C^5), 136.8 (d, $^1J_{CP}$ = 179, C^4), 126.5 (d, $^2J_{CP}$ = 7, C^3), 66.4 (CH_2O), 63.8 (d, $^2J_{PH}$ = 6, $POCH_2$), 36.0 ($\underline{C}(CH_3)_3$), 31.6 ($C(\underline{C}H_3)$), 21.0 (CH_3), 16.3 (d, $^3J_{PH}$ = 6, $POCH_2\underline{C}H_3$); ESI-LRMS (+) *m/z* 344.2 $[M+H]^+$; ESI-HRMS (+) calcd for $[C_{16}H_{27}NO_5P]^+$ 344.1627, found 344.1628.

Diethyl [5-*tert*-butyl-2-(hydroxymethyl)pyridin-4-yl]phosphonate

[5-*tert*-Butyl-4-(diethoxyphosphoryl)pyridin-2-yl]methyl acetate (300 mg, 0.87 mmol) was dissolved in anhydrous EtOH (4 mL) and purged with argon for 10 min, before sodium metal (~15 mg) was added. The resulting solution was stirred at rt for 1 h, under an atmosphere of argon. The solvent was removed under reduced pressure and the residue dissolved in CH_2Cl_2 (7 mL) and washed with H_2O (2 mL), before the aqueous layer was re-extracted with CH_2Cl_2 (3 × 7 mL). The organic layers were combined, dried over $MgSO_4$ and the solvent removed under reduced pressure. The resulting brown oil was purified by silica gel column chromatography, eluting with a gradient starting from 100% CH_2Cl_2 to 2% MeOH/ CH_2Cl_2, to yield a yellow oil (150 mg, 57%). R_f (10% MeOH/ CH_2Cl_2) = 0.48; ^{1}H NMR (400 MHz, $CDCl_3$) δ 8.80 (d, $^4J_{HP}$ = 8, 1H, H^6), 7.79 (d, $^3J_{HP}$ = 15, 1H, H^3), 4.80 (s, 2H, CH_2), 4.07-4.14 (m, ^3J = 7_{HP}, 4H, $POCH_2$), 2.58 (br s, OH), 1.59 (s, 9H, $C(CH_3)_3$), 1.35 (t, ^4J = 7_{HP}, 6H, $POCH_2C\underline{H}_3$); ^{31}P NMR (162 MHz, $CDCl_3$) δ 15.8-16.2 (m, $^3J_{PH}$ = 7); ^{13}C NMR (176 MHz, $CDCl_3$) δ 157.3 (d, $^3J_{CP}$ = 11, C^6), 148.1 (d, $^3J_{CP}$ = 13, C^2), 146.7 (d, $^2J_{CP}$ = 11, C^5), 136.5 (d, $^1J_{CP}$ = 179, C^4), 125.3 (d, $^2J_{CP}$ = 7, C^3), 64.2 (CH_2O), 62.7 (d, $^2J_{PH}$ = 6, $POCH_2$), 35.8 (d, $^3J_{CP}$ = 3, $\underline{C}(CH_3)_3$), 31.6 ($C(\underline{C}H_3)$), 16.3 (d, $^3J_{PH}$ = 6, $POCH_2\underline{C}H_3$); ESI-LRMS (+) *m/z* 302.2 $[M+H]^+$; ESI-HRMS (+) calcd for $[C_{14}H_{25}NO_4P]^+$ 302.1521, found 302.1519.

[5-*tert*-Butyl-4-(diethoxyphosphoryl)pyridin-2-yl]methyl methane sulfonate

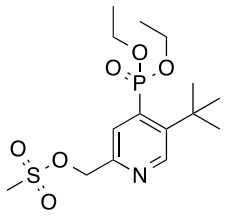

Diethyl [5-*tert*-butyl-2-(hydroxymethyl)pyridin-4-yl]phosphonate (150 mg, 0.50 mmol) was dissolved in anhydrous THF (4 mL) and cooled to 5 °C. Triethylamine (140 μL, 1.00 mmol) and methanesulphonyl chloride (58 μL, 0.75 mmol) were added dropwise and the resulting solution was stirred at rt for 30 min. The solvent was removed under reduced pressure before the residue was treated with brine (5 mL) and extracted with CH_2Cl_2 (3 × 10 mL). The organic layers were combined, dried over $MgSO_4$, and the solvent removed under reduced pressure to yield a pale orange oil, which was used immediately (176 mg, 93%). R_f (10% MeOH/ CH_2Cl_2) = 0.56; ^{1}H

NMR (400 MHz, $CDCl_3$) δ 8.78 (d, $^4J_{HP}$ = 8, 1H, H^6), 7.84 (d, $^3J_{HP}$ = 15, 1H, H^3), 5.26 (s, 2H, CH_2), 4.06-4.16 (m, $^3J_{HP}$ = 6, 4H, $POCH_2$), 3.05 (s, 3H, CH_3), 1.52 (s, 9H, $C(CH_3)_3$), 1.29 (dt, $^3J_{HP}$ = 6, $^4J_{HP}$ = 1, 6H, $POCH_2C\underline{H}_3$); ^{31}P NMR (162 MHz, $CDCl_3$) δ 15.4-15.8 (m, $^3J_{PH}$ = 6); ESI-LRMS (+) *m/z* 380.5 $[M+H]^+$; ESI-HRMS (+) calcd for $[C_{15}H_{27}NO_6PS]^+$ 380.1297, found 380.1302.

1,4,7-Tri-benzyl 1,4,7,10-tetraazacyclododecane 1,4,7-tricarboxylate

1,4,7,10-Tetraazacyclododecane (2.5 g, 14.5 mmol) was dissolved in dry CH_2Cl_2 (80 mL) and to this was added triethylamine (6.3 mL, 45.0 mmol). The resulting solution was stirred at 5 ºC for 10 min, before the dropwise addition of a solution of benzyl chloroformate (6.4 mL, 45.0 mmol) in dry CH_2Cl_2 (20 mL). After addition, the solution was stirred at rt for a further 18 h. The solvent was removed under reduced pressure and the resulting pale yellow oil was purified by silica gel column chromatography, eluting with a gradient starting from 100% CH_2Cl_2 to 2% MeOH/ CH_2Cl_2 to yield a colourless oil (6.1 g, 73%). R_f (10% MeOH/ CH_2Cl_2) = 0.54; ^1H NMR (400 MHz, $CDCl_3$) δ 7.22-7.33 (m, 15H, ArH), 5.00-5.06 (m, 6H, CH_2O), 3.63-3.67 (m, 2H, cyclen CH_2), 3.16-3.55 (m, 12H, cyclen CH_2), 2.75-2.92 (m, 2H, cyclen CH_2); ^{13}C NMR (101 MHz, $CDCl_3$) δ 156.1 (CO), 136.4 (Ar), 136.3 (Ar), 128.4 (Ar), 128.3 (Ar), 127.7 (Ar), 127.6 (Ar), 127.4 (Ar), 67.2 (CH_2O), 66.8 (CH_2O), 53.5 (cyclen CH_2), 50.6 (cyclen CH_2), 50.3 (cyclen CH_2), 50.2 (cyclen CH_2), 50.1 (cyclen CH_2), 45.6 (cyclen CH_2); ESI-LRMS (+) *m/z* 575.1 $[M+H]^+$; ESI-HRMS (+) calcd for $[C_{32}H_{39}N_4O_6]^+$ 575.2870, found 575.2867.

1,4,7-Tri-benzyl 10-*tert*-butyl 1,4,7,10-tetraazacyclododecane 1,4,7,10-tetracarboxylate

1,4,7-Tri-benzyl 1,4,7,10-tetraazacyclododecane 1,4,7-tricarboxylate (1.3 g, 2.26 mmol) was dissolved in dry CH_2Cl_2 (15 mL) and triethylamine added (0.4 mL, 2.94 mmol). The resulting solution was stirred at rt for 10 min, before adding di-*tert*-butyl dicarbonate (0.64 g, 2.94 mmol). The resulting solution was stirred at rt for 18 h before the solvent was removed under reduced pressure. The resulting yellow oil was purified by silica gel column chromatography, eluting with a gradient starting from 100% CH_2Cl_2 to 2% MeOH/ CH_2Cl_2 to yield a colourless oil (1.3 g, 85%). R_f (10%

MeOH/ CH_2Cl_2) = 0.69; ^{1}H NMR (400 MHz, $CDCl_3$) δ 7.21-7.34 (m, 15H, ArH), 5.06 (s, 2H, CH_2O), 5.03 (s, 4H, CH_2O), 3.00-3.54 (br m, 16H, cyclen CH_2), 1.36 (s, 9H, $C(CH_3)_3$); ^{13}C NMR (101 MHz, $CDCl_3$) δ 156.8 (CO), 136.4 (Ar), 128.6 (Ar), 128.4 (Ar), 128.3 (Ar), 128.2 (Ar), 82.8 ($\underline{C}(CH_3)_3$), 67.3 (CH_2O), 49.9-50.7 (br, cyclen CH_2), 28.4 ($C(\underline{C}H_3)_3$); ESI-LRMS (+) *m/z* 675.1 $[M+H]^+$; ESI-HRMS (+) calcd for $[C_{37}H_{47}N_4O_8]^+$ 675.3394, found 675.3406.

tert-Butyl-1,4,7,10-tetraazacyclododecane carboxylate

1,4,7-Tri-benzyl 10-*tert*-butyl 1,4,7,10-tetraazacyclododecane 1,4,7,10-tetracarboxylate (1.3 g, 1.93 mmol) was dissolved in MeOH (25 mL) and to this was added $Pd(OH)_2/C$ (~200 mg). The reaction vessel was loaded onto a Parr hydrogenator, where it was subject to agitation for 18 h, under a pressure of 40 bar H_2. The catalyst was filtered through Celite and the solvent was removed under reduced pressure. The resulting solid was washed with a minimum amount of NaOH (aq. solution, 1 mL), and extracted into CH_2Cl_2 (3 × 30 mL), before the organic layers were combined, dried over $MgSO_4$, and the solvent removed under reduced pressure to yield a pale yellow oil (0.52 g, 99%). ^{1}H NMR (400 MHz, CD_3OD) δ 5.03 (br s, NH), 3.52-3.60 (m, 4H, cyclen CH_2), 3.22-3.27 (m, 4H, cyclen CH_2), 3.10-3.21 (m, 8H, cyclen CH_2), 1.49 (s, 9H, $C(CH_3)_3$); ^{13}C NMR (101 MHz, CD_3OD) δ 157.5 (CO), 82.3 ($\underline{C}(CH_3)_3$), 48.2 (cyclen CH_2), 46.9 (cyclen CH_2), 45.6 (cyclen CH_2), 44.5 (cyclen CH_2), 28.7 ($C(\underline{C}H_3)_3$); ESI-LRMS (+) *m/z* 273.2 $[M+H]^+$; ESI-HRMS (+) calcd for $[C_{13}H_{29}N_4O_2]^+$ 273.2291, found 273.2296.

tert-Butyl-4,7,10-tri{[ethoxy(methyl)phosphoryl]methyl}-1,4,7,10-tetraazacyclododecane-1-carboxylate

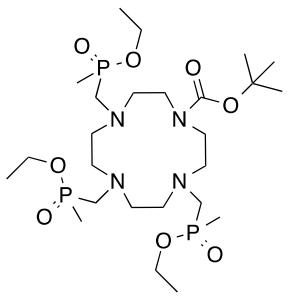

tert-Butyl-1,4,7,10-tetraazacyclododecane carboxylate (0.52 g, 1.91 mmol) and paraformaldehyde (1.15 g, 38.2 mmol) were dissolved in anhydrous THF (30 mL) and the resulting suspension was heated at 80 ^{o}C for 3 h. Diethyl methylphosphonite (1.7 mL, 11.5 mmol) was added and the solution stirred at 80 ^{o}C for a further 18 h. The solution was cooled and filtered, before the solvent was removed under reduced pressure. The residual brown oil was purified by alumina gel column chromatography, eluting with a gradient starting from 100% CH_2Cl_2 to 2% MeOH/ CH_2Cl_2 to yield a pale yellow oil (0.4 g, 33%). R_f (10% MeOH/ CH_2Cl_2) = 0.76; ^{1}H NMR (400 MHz, $CDCl_3$) δ 3.93 (q, $^{3}J_{PH}$ = 7, 6H, $POCH_2$), 3.09-3.60 (br m, 6H, PCH_2N), 2.41-3.00 (br m, 16H, cyclen CH_2), 1.33-1.47 (m, 9H, PCH_3), 1.32 (s, 9H, $C(CH_3)_3$), 1.18 (t, $^{3}J_{PH}$ = 7, 9H, $POCH_2C\underline{H}_3$); ^{31}P NMR (162 MHz, $CDCl_3$) δ 52.53, 52.31, 52.22, 52.20, 52.18, 52.24, 52.06, 51.95, 51.85, 51.85, 51.59, 51.49 (mixture of isomers); ^{13}C NMR (176 MHz, $CDCl_3$) δ 155.5 (CO), 79.5 ($\underline{C}(CH_3)_3$), 59.9-60.1 (m, $POCH_2$), 52.7-55.1 (m, cyclen CH_2), 45.9 (PCH_2N), 45.6 (PCH_2N), 45.5 (PCH_2N), 28.4 ($C(\underline{C}H_3)_3$), 16.6 (t, $^{3}J_{CP}$ = 6, $POCH_2\underline{C}H_3$), 13.5-13.9 (m, PCH_3); ESI-LRMS (+) *m/z* 633.2 $[M+H]^+$; ESI-HRMS (+) calcd for $[C_{25}H_{56}N_4O_8P_3]^+$ 633.3311, found 633.3312.

Ethyl[(4,7-di{[ethoxy(methyl)phosphoryl]methyl}-1,4,7,10-tetraazacyclododecane-1-yl)methyl](methyl)phosphinate

tert-Butyl-4,7,10-tri{[ethoxy(methyl)phosphoryl]methyl}-1,4,7,10-tetraazacyclododecane-1-carboxylate (0.4 g, 0.63 mmol) was dissolved in anhydrous CH_2Cl_2 (2 mL) and TFA added (2 mL). The resulting solution was stirred at rt for 18 h, before the solvent was removed under reduced pressure. The resulting yellow oil was dissolved in a minimal amount of H_2O (3 mL). The pH of the water layer was adjusted to 12 using solid NaOH before being extracted with CH_2Cl_2 (4 × 10 mL). The CH_2Cl_2 layers were combined, dried over $MgSO_4$, and the solvent removed under reduced pressure to yield a pale yellow oil (0.22 g, 66%). ^{1}H NMR (400 MHz, $CDCl_3$) δ 3.90-4.08 (m, 6H, $POCH_2$), 2.60-3.32 (br m, 22H, cyclen CH_2, PCH_2N), 1.46 (d, $^{2}J_{PH}$ = 13, 9H, PCH_3), 1.25 (t, $^{3}J_{PH}$ = 7, 9H, $POCH_2C\underline{H}_3$); ^{31}P NMR (162 MHz, $CDCl_3$) δ 54.2, 53.8, 53.5, 53.2, 50.4 (mixture of isomers); ^{13}C NMR (101 MHz, $CDCl_3$) δ 60.1-60.6 (m, $POCH_2$), 56.2-56.6 (m, cyclen CH_2), 55.1-55.5 (m, cyclen CH_2), 52.5-53.2 (m, cyclen CH_2), 46.8-47.3 (m, PCH_2N), 16.7 (t, $^{3}J_{CP}$ = 6,

$POCH_2\underline{C}H_3$), 14.2 (t, $^1J_{CP}$ = 12, $P\underline{C}H_3$), 13.3 (t, $^1J_{CP}$ = 12, $P\underline{C}H_3$); ESI-LRMS (+) *m/z* 533.1 $[M+H]^+$; ESI-HRMS (+) calcd for $[C_{20}H_{48}N_4O_6P_3]^+$ 533.2787, found 533.2811.

Diethyl {5-*tert*-butyl-2-[(4,7,10-tri{[ethoxy(methyl)phosphoryl]methyl}-1,4,7,10-tetraazacyclododecan-1-yl)methyl]pyridin-4-yl}phosphonate

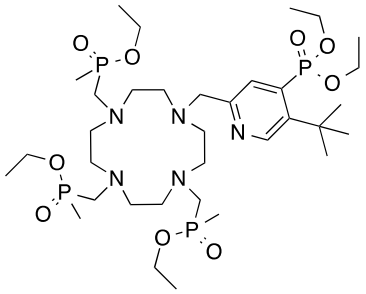

Ethyl[(4,7-di{[ethoxy(methyl)phosphoryl]methyl}-1,4,7,10-tetraazacyclododecane-1-yl)methyl](methyl)phosphinate (540 mg, 1.42 mmol) was dissolved in anhydrous MeCN (5 mL) and anhydrous K_2CO_3 added (196 mg, 1.42 mmol). [5-*tert*-Butyl-4-(diethoxyphosphoryl)pyridin-2-yl]methyl methanesulfonate (500 mg, 0.94 mmol) was then added dropwise as a solution in anhydrous MeCN (10 mL). The resulting mixture was heated at 70 ºC for 18 h, under argon. The reaction mixture was cooled and the inorganic salts were removed by centrifugation. The solvent was removed under reduced pressure and the resulting reddish oil was purified by alumina gel column chromatography, eluting with a gradient starting from 100% CH_2Cl_2 to 2% MeOH/ CH_2Cl_2 to yield a pale orange oil (210 mg, 27%). R_f (10% MeOH/ CH_2Cl_2) = 0.65; ^{1}H NMR (400 MHz, $CDCl_3$) δ 8.73 (d, $^4J_{HP}$ = 8, 1H, H^6), 7.88 (d, $^3J_{HP}$ = 16, 1H, H^3), 4.09-4.16 (m, 4H, $POCH_2$), 3.93-4.05 (m, 6H, $POCH_2$), 3.50-3.74 (m, 8H, NCH_2), 2.53-3.49 (br m, 16H, cyclen CH_2), 1.39-1.54 (m, 18H, $C(CH_3)_3$, PCH_3), 1.20-1.32 (m, 15H, $POCH_2C\underline{H}_3$); ^{31}P NMR (162 MHz, $CDCl_3$) δ 53.5, 52.9, 52.5, 52.4, 52.3, 52.2, 52.0, 51.9, 51.7, 51.5 (NCH_2P, mixture of isomers), 16.6, 15.9, 14.4 (pyP, mixture of isomers); ^{13}C NMR (101 MHz, $CDCl_3$) δ 149.0 (C^2), 136.2 (C^5), 129.5 (C^6), 127.3 (C^4), 111.7 (C^3), 62.5-62.8 (m, $POCH_2$), 59.7-60.3 (m, $POCH_2$), 53.0-55.0 (m, PCH_2N, $pyCH_2$, cyclen CH_2), 36.3 ($\underline{C}(CH_3)_3$), 31.3 ($C(\underline{C}H_3)_3$), 16.6 (d, $^3J_{CP}$ = 6, $POCH_2\underline{C}H_3$), 16.2 (d, $^3J_{CP}$ = 6, $POCH_2\underline{C}H_3$), 13.0-14.9 (m, $P\underline{C}H_3$); ESI-LRMS (+) *m/z* 816.7 $[M+H]^+$; ESI-HRMS (+) calcd for $[C_{34}H_{70}N_5O_9P_4]^+$ 816.4124, found 816.4129.

Lanthanide(III) complexes of {5-*tert*-butyl-2-[(4,7,10-tri{[hydroxy(methyl)phosphoryl]methyl}-1,4,7,10-tetraazacyclododecan-1-yl)methyl]pyridin-4-yl}phosphonic acid, [HLn.L^1]

In general, diethyl {5-*tert*-butyl-2-[(4,7,10-tri{[ethoxy(methyl)phosphoryl]methyl}-1,4,7,10-tetraazacyclododecan-1-yl)methyl]pyridin-4-yl}phosphonate was dissolved in aqueous HCl (6 M) and stirred at 70 ^{o}C for 18 h. Complete ester cleavage was confirmed by ESI-MS (+) (LR: *m/z* 676.6 [M+H]+; HR: *m/z* calc for $[C_{24}H_{50}N_5O_9P_4]^+$ 676.2559, found 676.2557). The solvent was removed under reduced pressure and the resulting yellow oil was dissolved in H_2O (1 mL). The pH of the solution was adjusted to 5.5 using aqueous NaOH solution and $LnCl_3.6H_2O$ was added. The resulting solution was stirred at 70 C for 18 h before the solvent was removed under reduced pressure. The resulting yellow solid was purified by reverse-phase HPLC (10-100% MeOH in H_2O over 10 min) to yield a white solid.

[HEu.L^1]$^-$ t_R = 7.3 min; ^{1}H NMR (400 MHz, pD 7.4, $CDCl_3$) δ +3.1 ($C(CH_3)_3$ major), +1.4 ($C(CH_3)_3$ minor); ESI-LRMS (+) *m/z* 825.8 $[M+H]^+$; ESI-HRMS (+) calc. for $[C_{24}H_{47}N_5O_9P_4{}^{151}Eu]^+$ 824.1523, found 824.1549.

[HGd.L^1]$^-$ t_R = 7.1 min; ESI-LRMS (+) *m/z* 830.4 $[M+H]^+$; ESI-HRMS (+) calc. for $[C_{24}H_{47}N_5O_9P_4{}^{154}Gd]^+$ 827.1533, found 827.1561; r_{1p} = 2.0±0.05 mM^{-1} s^{-1} (H_2O, 60 MHz, 310 K).

[HTb.L^1]$^-$ t_R = 7.3; min; ^{1}H NMR (400 MHz, pD 7.4, $CDCl_3$) δ -78.3 ($C(CH_3)_3$ minor), -83.4 ($C(CH_3)_3$ major); ESI-LRMS (+) *m/z* 832.2 $[M+H]^+$; ESI-HRMS (+) calc. for $[C_{24}H_{47}N_5O_9P_4{}^{159}Tb]^+$ 832.1578, found 832.1562.

[HDy.L^1]$^-$ t_R = 6.9 min; ^{1}H NMR (400 MHz, pD 7.4, $CDCl_3$) δ -77.1 ($C(CH_3)_3$ major), -75.7 ($C(CH_3)_3$ minor); ^{31}P NMR (162 MHz, $CDCl_3$) δ -38.2 (pyP); ESI-LRMS (+) *m/z* 836.4 $[M+H]^+$; ESI-HRMS (+) calc. for $[C_{24}H_{47}N_5O_9P_4{}^{160}Dy]^+$ 833.1576, found 833.1573.

[HHo.L^1]$^-$ t_R = 7.1 min; ^{1}H NMR (400 MHz, pD 7.4, $CDCl_3$) δ -33.5($C(CH_3)_3$ major), -32.2 ($C(CH_3)_3$ minor); ESI-LRMS (+) *m/z* 836.2 $[M+H]^+$; ESI-HRMS (+) calc. for $[C_{24}H_{47}N_5O_9P_4{}^{165}Ho]^+$ 836.1471, found 836.1473.

[HEr.L^1]$^-$ t_R = 7.0 min; ^{1}H NMR (400 MHz, $CDCl_3$) δ +42.5 ($C(CH_3)_3$ major), +44.2 ($C(CH_3)_3$ minor); ESI-LRMS (+) *m/z* 840.1 $[M+H]^+$; ESI-HRMS (+) calc. for $[C_{24}H_{47}N_5O_9P_4{}^{164}Er]^+$ 837.1616, found 837.1636.

[HTm.L^1]$^-$ t_R = 6.9 min; ^{1}H NMR (400 MHz, $CDCl_3$) δ +74.6 ($C(CH_3)_3$ major), +75.5 ($C(CH_3)_3$ minor); ESI-LRMS (+) *m/z* 841.9 $[M+H]^+$; ESI-HRMS (+) calc. for $[C_{24}H_{47}N_5O_9P_4{}^{154}Tm]^+$ 842.1667, found 842.1647.

MRI methodology for PARASHIFT measurements

In vitro and *in vivo* imaging was performed using a 7T preclinical MRI system (20cm bore, Varian Direct Drive scanner, Agilent, Palo Alta, CA) equipped with a 30mm i.d. quadrature birdcage RF coil (Rapid Biomedical GmbH, Germany) for excitation and detection of the water and PARASHIFT agent signals.

Imaging measurements were developed using the excitation bandwidth and offset frequencies of the RF pulses together with the receiver spectral width to limit the MRI detection to individual resonances (water or either of the PARASHIFT probe reported frequencies). The short T_1 times for the *tert*-butyl resonances allows very short imaging repetition times (TR) at high flip angle and enables high numbers of signal averages to be acquired to maximize signal to noise ratio while maintaining practical total scan durations. Optimal flip angle (Ernst angle) can also be defined *a* priori since the PARASHIFT R_1 is known and fixed by the *intramolecular* interaction with the Ln ion, independent of tissue concentration.

Two types of scan acquisition were used – 3 dimensional gradient echo (3D-GE) imaging and 2 dimensional spectroscopic imaging (2DSI), which were applied either for imaging single resonances or for triple frequency imaging. In every case, the excitation RF pulse was a 500 μs duration Gaussian modulated pulse which has a FWHM bandwidth of 2100Hz, falling to a fractional excitation of $<10^{-3}$ at 20 kHz. This pulse specification allows separate excitation of water only, the *tert*-butyl group of $[Dy.HL^1]^-$ or $[Tm.HL^1]^-$ by varying the transmit frequency.

Single resonance images were acquired with the RF pulse at the appropriate excitation frequency and with a 20 kHz receiver bandwidth. The 3D-GE method was used for imaging the basic spatial distribution of the resonances. Other 3D-GE image acquisition parameters were: TR/TE 4.98/0.57ms, axial FOV 64×64mm, matrix 64×64 (1mm in-plane resolutioin), 16 encodes in the 3rd direction covering a slab thickness of 64mm yielding 4mm thick slices. Scans used 30 signal averages for a total duration of 152s per dataset. Pulse power was calibrated to the PARASHIFT

Ernst angle of 54°. A typical 3D-GE dataset in a multi-tube phantom containing $[Dy.HL^1]^-$ is shown in ESI Figure 1. The 2DSI method was used to acquire full spectra from a 2D grid of voxels across the object. From these spectra the shifts in frequency due to changes in T and pH could be measured. Sequence parameters for 2DSI were TR/TE =10.84/0.65 ms, FOV 64×64mm, matrix16×16 (4mm in-plane resolution), 512 data points. Scans used 30 signal averages with scan duration of 83s. The resulting data was 3 dimensional (2 spatial, 1 spectroscopic) with the spatial dimension localizing a thick axial (XY) plane condensing all detail along the Z direction of the magnet. Spectra extracted from a typical 2DSI dataset in a multi-tube phantom containing $[Dy.HL^1]^-$ are shown in ESI Figure 2.

Triple imaging (simultaneous but separate imaging of water, $[Dy.HL^1]^-$ and $[Tm.HL^1]^-$) was acquired using a novel pulse sequence. 3D-GE and 2DSI sequences were adapted to include two back-to-back RF pulses whose flip angle, excitation bandwidth and excitation frequency could be independently adjusted. For the experiments described here the two pulses were again 500 μs duration Gaussian pulses with equal flip angle (since R_1 values for both the $[Dy.HL^1]^-$ and $[Tm.HL^1]^-$ t-Bu resonaces were similar) tuned to the resonance frequencies of the $[Dy.HL^1]^-$ and $[Tm.HL^1]^-$ (approximately -23600 and 19900 Hz respectively). The bandwidth of these pulses does not extend to the water resonance (0 Hz), however in practice a small residual off-resonance excitation was present at the water frequency such that no explicit water excitation was needed for the triple imaging. For 3D-GE triple imaging signal detection was centred at the water frequency with data matrix trebled and imaging bandwidth trebled to 60KHz to simultaneous detect all 3 frequencies. The data matrix can then be equally divided into 3 in the readout (directly detected) direction, providing independent images of the 3 resonances. Other sequence parameters were $TR/TE_{1(Dy)}/TE_{2(Tm)}$ = 4.98/0.57/1.27ms, axial FOV 64×64mm, matrix 64×64 (1mm in-plane resolution), 16 encodes in the 3rd direction covering a slab thickness of 64mm yielding 4mm thick slices. Scans used 30 signal averages for a total duration of 152s per dataset. Pulse power was calibrated (using the water signal) to the PARASHIFT Ernst angle of 54°.

For triple imaging with 2DSI, spectral width was again set to 60 kHz with the number of sampled data points set at 512. Other sequence parameters were $TR/TE_{1(Dy)}/TE_{2(Tm)}$ =10.84/0.65/1.65ms, axial FOV 64×64mm, matrix 16×16 (4mm in-plane resolution).

Scans used 30 signal averages with scan duration of 83s. The resulting data was 3 dimensional (2 spatial, 1 spectroscopic) with the spatial dimension localizing a thick axial (XY) plane condensing all detail along the Z direction of the magnet.

***In vivo* triple imaging acquisitions**

Preliminary *in vivo* imaging studies were conducted in 3 CD1 wild type mice (Charles River, UK) to demonstrate dynamic triple imaging and non-invasive measurement of tissue temperature and pH. Mice were mounted in a dedicated bed including a pneumatic pillow system to measure animal respiration with a fiber-optic thermometry system for temperature monitoring and control via a warm air system (SA Instruments Inc., Stony Brook, NY). Mice were anaesthetized using isoflurane and an i.v. line was inserted into a tail vein to allow injection of contrast agent from outside of the magnet. Unlike many previous *in vivo* studies using i.v. injection of paramagnetically shifted agents, these animals were physiologically intact, i.e. without renal ligation. All animal experiments were performed complying with the UK Government Home Office under the animals (scientific procedure) act 1986. Animals were positioned in the birdcage coil with a phantom placed under the body of the animal but fastened to a line that allowed it to be withdrawn from the imaging FOV following calibration to avoid contamination of the *in vivo* signal from the phantom. This phantom consisted of a 5 mm diameter NMR tube phantom containing ~100μL of 4mM solution of the two PARASHIFT agents at pH of 7.0, surrounded by a concentric tube containing ethylene glycol as a NMR temperature reference. To confirm animal positioning and visualize regional anatomy conventional spin-echo MRI scans were collected on the water resonance (TR/TE=1000/14.56ms, 40 × 1mm thick slices, field of view FOV 40 × 40mm, matrix 256 × 256).

Following flip angle calibration, a triple imaging 2DSI data acquisition was then collected in the axial plane from which the phantom temperature and frequency of each PARASHIFT resonance could be determined. The phantom was then withdrawn from the field of view and a further 2DSI dataset collected which showed only the intrinsic water (and fat) resonance from the animal. A dynamic series of triple imaging 3DGE and 2DSI acquisitions were then collected commencing with the injection of 200μl of a mix of the two PARASHIFT agents (0.04 mmol/kg each of $[Dy.HL^1]^-$ and $[Tm.HL^1]^-$), followed by saline flush and continuing for 30 minutes.

Acknowledgements We thank the ERC (FCC 266804) and EPSRC (EP/ L01212X/1) for generous support.

Key Words Triple imaging; MRI; lanthanide; pH; spectral imaging

References

[1] M. D. Fox and M. E. Raichle, *Nature Rev. Neurosci*. **2007**, *8*, 700-711.

[2] N. Houssami, S. Ciatto, P. Macaskill, S. J. Lord, R. M. Warren, J. M. Dixon and L. Irwig, *J. Clin. Oncol*. **2008**, *26*, 3248-3258.

[3] J. V. Frangioni, *J. Clin. Oncol*. 2008, **26**, 4012-4021; T. B. Rodriguez, E. M. Sarrao, B. W. C. Kennedy, D-E. Hu, M. I. Kettunen and K. M. Brindle, *Nature Med*. **2014**, *20*, 93-97.

[4] P. K. Senanayake, N. J. Rogers, P. Harvey, K-L. N. A. Finney, A. M. Funk, D. Parker, J. I. Wilson, R. Maxwell and A. M. Blamire, *Magn. Reson. Med*. **2017**, *77*, 1307-1317.

[5] P. Harvey, A. M. Blamire, J. I. Wilson, K-L. N. A. Finney, A. M. Funk, P. K. Senanayake, D. Parker, *Chem. Sci.* **2013**, *4,* 4251.

[6] a) K. H. Chalmers, A. M. Kenwright, D. Parker, A. M. Blamire, *Magn. Reson. Med*. **2011**, *66*, 931-936; b) R. Schmidt, C. Holtke, D. Parker and C. Faber, *Magn. Reson. Med.* **2013**, *69*, 1056; c) R. Schmidt, N. Nippe, K. Strobel, M. Masthoff, O. Reifschneider, D. D. Castelli, C. Holtke, S. Aime, U. Karst,, C. Sunderkotter, C. Bremer, C. Faber, *Radiology*, **2014**, *272*, 785-795.

[7] A. M. Funk, K-L. N. A. Finney, P. Harvey, A. M. Kenwright, E. R. Neil, N. J. Rogers, P. K. Senanayake and D. Parker, *Chem. Sci.* **2015**, *6,* 1655.

[8] a) A. M. Funk, P. Harvey, K-L. N. A. Finney, M. A. Fox, A. M. Kenwright, N. J. Rogers, P. K. Senanayake and D. Parker, *Phys. Chem. Chem. Phys*. **2015**, *17*, 16507; b) A. M. Funk, P. Fries, A. M. Kenwright, P. Harvey and D. Parker, *J. Phys. Chem. A*, **2013**, *117*, 905-917; c) N. J. Rogers, K-L. N. A. Finney, P. K. Senanayake, D. Parker, *Phys. Chem. Chem. Phys*. **2016**, *18*, 4370.

[9] S. Aime, M. Botta, M. Fasano and E. Terreno, *Chem. Soc. Rev.* **1998**, *27*, 19-29.

[10] (a) A. M. Kenwright, I. Kuprov, E. De Luca, D. Parker, S. U. Pandya, P. K. Senanayake, D. G. Smith, *Chem. Commun*. **2008**, *22*, 2514; (b) P. K. Senanayake, A. M. Kenwright, D. Parker and S. K. van der Hoorn, *Chem. Comm.*, **2007**, 2923–2925.

[11] (a) N. McVicar, A. X. Li, M. Suchy, R. H. E Hudson, R. S. Menon, R. Bartha, *Magn. Reson. Med.* **2013**, *70*, 1016-1025; b) N Raghunand, C Howison, AD Sherry, S Zhang, RJ Gillies, Magn. Reson. Med. **2003**, *49*, 249; (c) D. L. Longo, A. Busato, S. Lanzardo, F. Antico, S. Aime, *Magn. Reson. Med*. **2012**, *70*, 859-864; (d) using Iopamidol for CEST

analysis of urine: A. Müller-Lutz, N. Khalil, B. Schmitt, V. Jellus, G. Pentang, G. Oeltschner, G. Antoch, R. S. Lanzman, H-J. Wittsack, *Magn. Reson. Mater. Phy.* **2014**, *27*, 477; (e) L. Q. Chen, C. M. Howison, J. J. Jeffery, I. F. Robey, P. H. Kuo, M. D. Pagel *Magn. Reson. Med.* **2014**; *72(5):* 1408–1417.

[12] R. B. Moon and J. H. Richards, *J. Biol. Chem*. **1973**, *248*, 7276-7278; R. J. Gillies, Z. Liu and Z. Bhujwalla, *Am. J. Physiol. Chem. Physiol*. **1994**, *36*, 195-203.

[13] D. M. Doddrell, W. M. Brooks, J. M. Bulsing, J. Field, M. G. Irving and H. Baddeley, *J. Magn. Reson*. **1986**, *68*, 367-372.

[14] D. Coman, H. K. Trubel, F. Hyder, *NMR Biomed.*, **2010**, *23*, 277-285.

[15] (a) D. Coman, R. A. de Graaf, D. L. Rothman and F. Hyder, *NMR Biomed*. **2013**, *26*, 1589-1593; (b) Y. Huang, D. Coman, P. Herman, J. U. Rao, S. Maritim, F. Hyder, *NMR Biomed.* **2016**, *29* 1364-1372.

[16] D. Villemin, A. Elbilali, F. Simeon, P. A. Jaffres, G. Maheut, M. Mosaddak and A. Hakiki, *J. Chem. Research (S)*, **2003**, 436–437.

[17] O. A. Blackburn, R. M. Edkins, S. Faulkner, A. M. Kenwright, D. Parker, N. J. Rogers, S. Shuvaev, *Dalton Trans.* **2016**, *45*, 6782-6800.

[18] a) S. Aime, M. Botta, D. Parker and J. A. G. Williams, *Dalton Trans*. **1995**, 2259; b) K. Mason, N. J. Rogers, E. Suturina, J. A. Aguilar, D. S. Yufit, A. S. Batsanov and D. Parker, *Inorg. Chem*. **2017**, *56*, 4028-4038.

[19] I. Bertini, C. Luchinat, G. Parigi, *Prog. Nucl. Mag.Reson. Spectrosc*. **2002**, *40*, 249-273.

[20] A. J. Vega and D. Fiat, *Mol. Phys*. **1976**, *31***,** 347.